Discrepancies between MODIS and ISCCP land surface temperature products analyzed with microwave measurements

Jean-Luc Moncet,[1] Pan Liang,[1] Alan E. Lipton,[1] John F. Galantowicz,[1] and Catherine Prigent[2]

Received 2 December 2010; revised 25 August 2011; accepted 26 August 2011; published 4 November 2011.

[1] This paper compares land surface temperature (LST) products from the Moderate Resolution Imaging Spectroradiometer (MODIS) and the International Satellite Cloud Climatology Project (ISCCP). With both sources, the LST data are derived from infrared measurements. For ISCCP, LST is a secondary product in support of the primary cloud analyses, but the LST data have been used for several other purposes. The MODIS measurements from the Aqua spacecraft are taken at about 01:30 and 13:30 local time, and the ISCCP three-hourly data, based on several geostationary and polar orbiting satellites, were interpolated to the MODIS measurement times. For July 2003 monthly averages over all clear-sky locations, the ISCCP-MODIS differences were +5.0 K and +2.5 K for day and night, respectively, and there were areas with differences as large as 25 K. The day–night differences were as much as ~10 K higher for ISCCP than for MODIS. The MODIS measurements were more consistent with independent microwave measurements from AMSR-E, by several measures, with respect to day–night differences and day-to-day variations.

Citation: Moncet, J.-L., P. Liang, A. E. Lipton, J. F. Galantowicz, and C. Prigent (2011), Discrepancies between MODIS and ISCCP land surface temperature products analyzed with microwave measurements, *J. Geophys. Res.*, *116*, D21105, doi:10.1029/2010JD015432.

1. Introduction

[2] Global land surface temperature (LST) data sets have been produced from infrared measurements. In recent years, the more commonly used LST data sets include those from the Moderate Resolution Imaging Spectroradiometer (MODIS) [*Wan*, 1999, 2008] on Earth Observing System Terra and Aqua satellites and from the International Satellite Cloud Climatology Project (ISCCP) [*Rossow and Schiffer*, 1999]. The MODIS product has been used in estimation of surface long-wave radiation [*Wang et al.*, 2005] and in drought monitoring [*Wan et al.*, 2004a]. The ISCCP product has, for example, been used as a constraint on the LST in experimental land surface data assimilation [*Bosilovich et al.*, 2007] and for analysis of diurnal cycles of LST for climate studies [*Ignatov and Gutman*, 1999; *Aires et al.*, 2004].

[3] The MODIS LST product has been the subject of several validation studies [*Wan et al.*, 2004b; *Wan*, 2008; *Wan and Li*, 2008; *Coll et al.*, 2009], which indicate LST errors are generally <1 K. The ISCCP LST product has been validated only indirectly, in the context of its intended role in producing the validated ISCCP cloud products [*Rossow and Garder*, 1993a, 1993b].

[4] Our work on retrieval of microwave emissivities with the aid of MODIS and ISCCP LST data [*Moncet et al.* 2011] suggested that there are substantial discrepancies between the LST data from these two sources. In that work, the primary source of microwave measurements was the Advanced Microwave Scanning Radiometer for the Earth Observing System (AMSR-E). We retrieved emissivity from microwave measurements by solving the equation

$$T^B_{\nu,p} = \left(T^{\uparrow}_{\nu} + \tau_\nu T^{\downarrow}_{\nu}\right) + \varepsilon_{\nu,p}\left(\tau_\nu T_{eff,\nu} - \tau_\nu T^{\downarrow}_{\nu}\right), \qquad (1)$$

where $T^B_{\nu,p}$ is the brightness temperature at frequency ν and polarization p, τ_ν is the total atmospheric transmittance along the sensor line of sight and, $T^{\uparrow}_{\nu}$ and $T^{\downarrow}_{\nu}$ represent the upwelling and downwelling atmospheric emission, respectively, and $\varepsilon_{\nu,p}$ is the surface emissivity. In (1), $T_{eff,\nu}$ is the effective emission temperature of the surface. For moderately heavily vegetated and moist surfaces, we make the approximation that $T_{eff,\nu}$ is approximately equal to the surface skin temperature, which we estimate from the LST retrieved from clear-sky infrared measurements. In areas that are dry and sparsely vegetated, where the measurements are affected by microwave radiation penetrating from sub-surface soil layers, we obtain $T_{eff,\nu}$ by applying the one-dimensional heat flow equation for a time series of measurements that spans one or more diurnal cycles.

[5] In places and periods of time where the emissivity-related characteristics of the surface (vegetation, moisture, etc.) are stable, the retrieved emissivities are stable also,

[1]Atmospheric and Environmental Research, Lexington, Massachusetts, USA.
[2]Laboratoire d'Etudes du Rayonnement et de la Matière en Astrophysique, Observatoire de Paris, CNRS, Paris, France.

Copyright 2011 by the American Geophysical Union.
0148-0227/11/2010JD015432

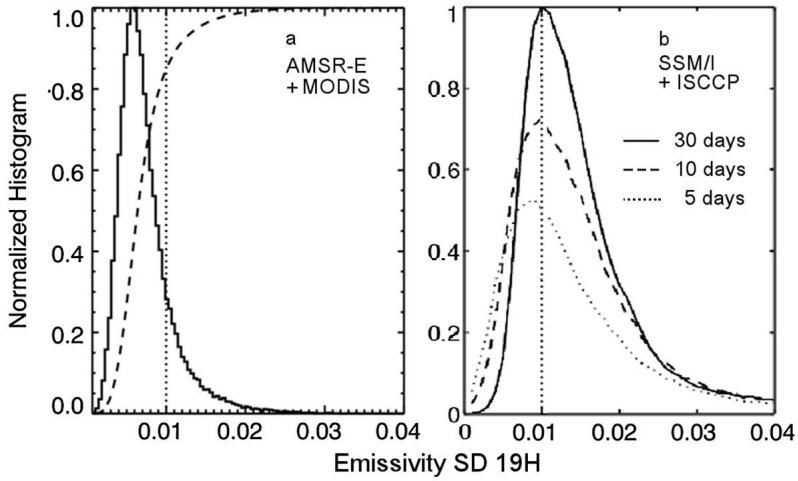

Figure 1. Normalized histograms of the ESD at 19H from (a) AMSR-E and MODIS, and (b) SSM/I and ISCCP. The AMSR-E ESD are for July 2003, and are limited to clear areas ($F_{clear} \geq 98\%$) with stable surface properties (R11 standard deviation < 0.01), where F_{clear} and R11 are defined in sections 2 and 4, respectively. Nighttime results are shown, while daytime results are similar. The SSM/I ESD are given for periods of 5, 10 and 30 days for July 1994 [*Prigent et al.*, 2006]. The 30-day histograms are normalized to 1 at maximum.

except to the extent there are errors in the retrieval input data that may vary from day-to-day. *Moncet et al.* [2011] analyzed the stability of retrieved emissivities in terms of their standard deviation over a one month period. When restricting the analysis to locations with stable surface properties and minimal cloud cover, and using MODIS LST for $T_{eff,\nu}$, we found that 91% of locations had emissivity standard deviations (ESDs) < 0.01 in the 19-GHz horizontal-polarization (19H) channel, for data from July 2003 (Figure 1a). This high temporal stability of the retrieved 19-GHz AMSR-E emissivities contrasts with the histograms presented by *Prigent et al.* [2006] for July 1994 (Figure 1b), for which only about 30% of grid points had $ESD_{19H} < 0.01$. Those 1994 retrievals, which we considered as heritage for our work, were derived from Special Sensor Microwave/Imager (SSM/I) data with LST from ISCCP. The fact that the analyses from AMSR-E focused on homogeneous and temporally stable surfaces accounts for some of this difference, but it does not explain all of it. The desire to maintain continuity (and consistency) with the SSM/I product, combined with the fact that SSM/I brightness temperatures are used in the generation of our emissivities for dry areas (the time series approach), prompted us to perform a comparison of the AMSR-E and SSM/I emissivities. Results presented in this paper suggest that the LST data quality was the primary reason for the histogram differences shown in Figure 1. In section 3, we summarize the differences between MODIS and ISCCP LST products for the month of July 2003. In order to get some insight into the quality of the ISCCP and MODIS LSTs, we compared the surface emissivities retrieved from the AMSR-E measurements using both ISCCP and MODIS LST as estimates of $T_{eff,\nu}$, in term of their temporal stability and spatial coherence. The results of this analysis which are presented in section 4 demonstrate the potential of using such microwave-based technique (even though its application is restricted to homogeneous stable surfaces) in assessing the quality of remotely sensed (or modeled) land surface products.

2. Data and Preprocessing

[6] Here we overview essential aspects of the data and its preparation for the analyses covered in this paper. Additional details about the data and processing applied to extract microwave emissivities are provided by *Moncet et al.* [2011]. The analyses reported here used global land data from July 2003.

[7] The microwave analyses presented here also focused on clear-sky conditions, in part because it was not possible to correct the microwave measurements for the impact of clouds with sufficient accuracy for these comparisons, but also because, in partly cloudy conditions, there would be an inherent mismatch between an average LST over a microwave footprint and an infrared-derived average from the clear portions only. This requirement combined with the need to restrict ourselves to homogeneous areas with temporally stable microwave surface properties (section 4) obviously results in a loss in spatial coverage, but the retained data covers enough regions with different surface types to enable us to perform meaningful cross-sensor validation and detect potential issues related to the production of clear-sky LST estimate from IR measurements (i.e., treatment of surface emissivity, atmospheric correction, and calibration).

[8] MODIS LST data and cloud flags were from Version 4 of the 5-km Level-3 gridded MYD11B1 product from the MODIS day/night algorithm [*Wan*, 1999, 2008]. The MODIS day/night LST algorithm relies on surface emissivity being stable over periods of a few days to simultaneously retrieve clear-sky LST, air temperature and column water vapor for day and night, and surface emissivities in 7 MODIS bands (20, 22, 23, 29, 31, 32 and 33) from a set of 14 clear daytime and nighttime measurements at a same location. The algo-

rithm uses the MODIS cloud mask for clear-pixel identification. Additional filtering is applied to reduce residual cloud contamination [*Moncet et al.*, 2011]. Here, we used data from the Aqua platform, with ascending and descending nominal equator crossing times (ECT) 13:30 and 01:30 local, because of the excellent time collocation with the AMSR-E observations.

[9] For ISCCP LST we used the DX product, following *Prigent et al.* [1997], which is produced from polar and geostationary satellite measurements on a 30-km grid and is available at 3-h intervals [*Rossow and Schiffer*, 1999; *Rossow and Garder*, 1993a, 1993b]. In ISCCP, cloud parameters and surface skin temperature are retrieved from visible (0.6 μm) and infrared (11μm) radiances. Analysis of the infrared measurements includes identification of clear scenes and correction for atmospheric effects. Under clear sky conditions, the surface skin temperature is estimated, with the assumption of unit emissivity. The error associated with the surface temperature is estimated to follow a Gaussian distribution with zero mean and 4 K standard deviation [*Rossow and Garder*, 1993b]. A small surface-type dependent correction to the initial skin temperature estimates is applied to account for variations in the 11 μm surface emissivity, based on the database used in the GISS climate model [*Zhang et al.*, 2010].

[10] The microwave AMSR-E instrument shares the Aqua platform with MODIS, and has a conical scan pattern at an Earth incidence angle (EIA) of 55°. There are vertical (V) and horizontal (H)-polarized channels centered at 6.925, 10.65, 18.7, 23.8, 36.5, and 89 GHz [*Kawanishi et al.*, 2003], abbreviated here as 7, 11, 19, 24, 37, and 89 GHz, respectively. We used SSM/I measurements [*Hollinger et al.*, 1990; *Colton and Poe*, 1999] from flights F13 and F15 of the Defense Meteorological Satellite Program (DMSP), with nominal ascending node ECT 18:33 and 21:05, respectively. SSM/I has V and H-polarized channels at 19.35, 37, and 85.5 GHz and a V-polarized channel at 22.235 GHz. The nominal EIA is 53.1°. No infrared-derived LST information is available from the DMSP platforms.

[11] For microwave emissivity retrievals using (1), we computed τ_ν, $T_\nu^\uparrow$, and $T_\nu^\downarrow$ with a radiative transfer model [*Lipton et al.*, 2009] in which the atmospheric absorption was from *Rosenkranz* [1998] and *Liebe et al.* [1992]. The required atmospheric temperature and water vapor profiles were taken from the 1° National Centers for Environmental Prediction (NCEP) Global Data Assimilation System (GDAS) analysis [*Kanamitsu*, 1989; *Kalnay et al.*, 1990]. The 3-hourly NCEP product was interpolated to the local time of the microwave sensor overpass and to the center of each microwave footprint.

[12] When MODIS LST data were used for $T_{eff,\nu}$ in (1), the 5-km data were averaged to the microwave footprints with weighting from the AMSR-E common spatial response pattern. The degree of cloud contamination in a footprint was inferred from the LST quality flags, so that LST data with a claimed uncertainty < 3 K were assigned a quality flag of one and, flags were set to zero in all other instances, including situations where no LST estimate was produced, which includes cases for which MWIR bands 20 and 22 used by the MODIS day/night algorithm saturated over hot spots in arid areas. These instances with zero weight are thus excluded from our process. Applying the same spatial averaging process to the quality flags as was used for the LST data provided an estimate of the fraction of clear sky within the AMSR-E footprint, designated here as F_{clear}. A footprint was treated as "clear" when $F_{clear} \geq 98\%$.

[13] A similar process is applied to the ISCCP data. In this case, we did no explicit spatial averaging of the LST and clear flag (set to 1 when grid box is clear and to 0 when it is cloudy) because these data are available only in a pre-averaged form. When these data were used for $T_{eff,\nu}$ in (1), LST and clear flags were spatially interpolated to the center of the microwave footprint using a bilinear formula, which is effectively a weighted average. Unlike in the MODIS case, grids that contain no valid ISCCP LST estimate are ignored and the ISCCP data are interpolated from the remaining locations. Temporal matching of ISCCP LST data with MODIS LST or microwave data is done by linearly interpolating the ISCCP product to the time of the other data set to yield final LST estimate and F_{clear}. Interpolation errors are minimized by interpolating the more frequently sampled ISCCP data rather than the less frequently sampled other data.

3. Direct Comparison of MODIS and ISCCP LST

[14] Figure 2 shows the mean differences between ISCCP and MODIS LST for July 2003. In this case, the 5-km MODIS LST data were averaged over each ISCCP grid box, thereby avoiding errors due to spatial interpolation. Our comparisons of MODIS and ISCCP LST data were limited to days that were clear ($F_{clear} \geq 98\%$ per both MODIS and ISCCP cloud masks) at the scale of the ISCCP 30-km grid. The ISCCP LST values tend to be higher than those from MODIS for both day and night over arid and semi-arid areas. The nighttime global (clear) difference between ISCCP and MODIS has a mean +2.5 K and standard deviation of 2.5 K (Figure 3). Daytime differences exceed 20 K over the hottest regions of the Northern Hemisphere and over the Southern African continent. Differences between the day and night LST from the MODIS overpass times are only approximations of the diurnal cycle amplitude, because the diurnal maximum typically occurs in the early afternoon and the minimum occurs near dawn. This amplitude, which is a significant diagnostic parameter for heat flux climatology, is substantially larger for ISCCP than for MODIS over large areas of Africa and Asia (Figure 4).

[15] MODIS and ISCCP LST temporal standard deviations are comparable for night data (Figure 5), with values being slightly higher for ISCCP. Differences are much more striking for day data, where MODIS LSTs remain quite stable, with 92% of the grid points having a standard deviation less than 4 K (versus 97% at night), whereas this fraction drops to 65% for ISCCP. In ~5% of the clear areas, ISCCP LST standard deviations exceed 8 K, while none exceed that value for MODIS. The areas of highest ISCCP temporal standard deviations (Figure 6) broadly coincide with the areas of largest mean ISCCP-MODIS LST differences (Figure 2) although, based on examination of spatial patterns on regional scales, correlation between the two factors is low. There are also isolated regions (e.g., in Russia and Argentina) where both MODIS and ISCCP have high temporal standard deviations.

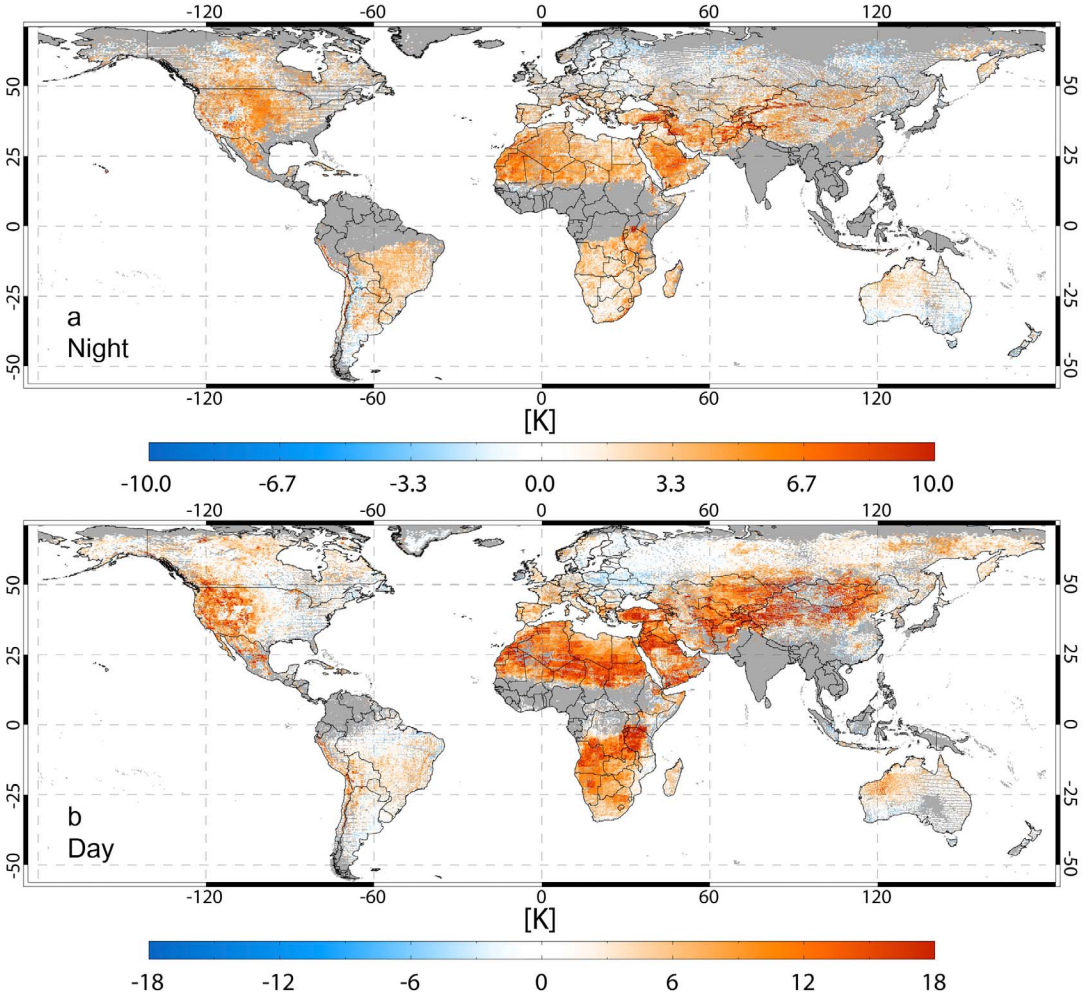

Figure 2. ISCCP-MODIS LST differences for July 2003 monthly mean at the time of (a) night and (b) day MODIS measurements, limited to clear conditions. The color scales are different on the two frames.

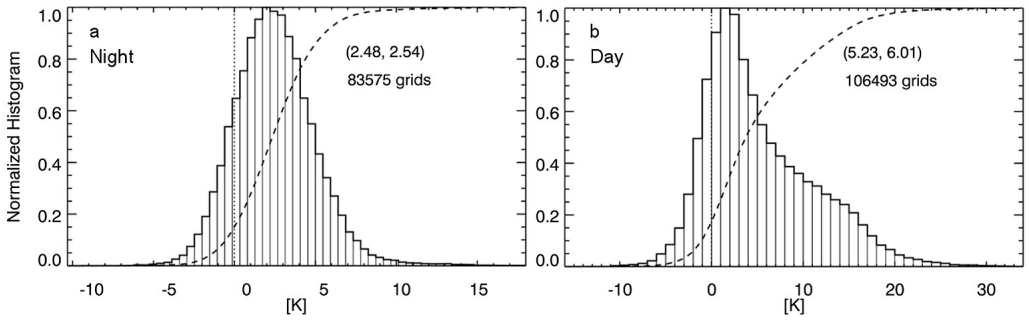

Figure 3. Histograms of ISCCP-MODIS LST differences for July 2003 monthly mean for (a) nighttime and (b) daytime, as in Figure 2. The horizontal axes are different in the two frames. The dashed lines are cumulative frequencies. The mean and standard deviation are in parentheses.

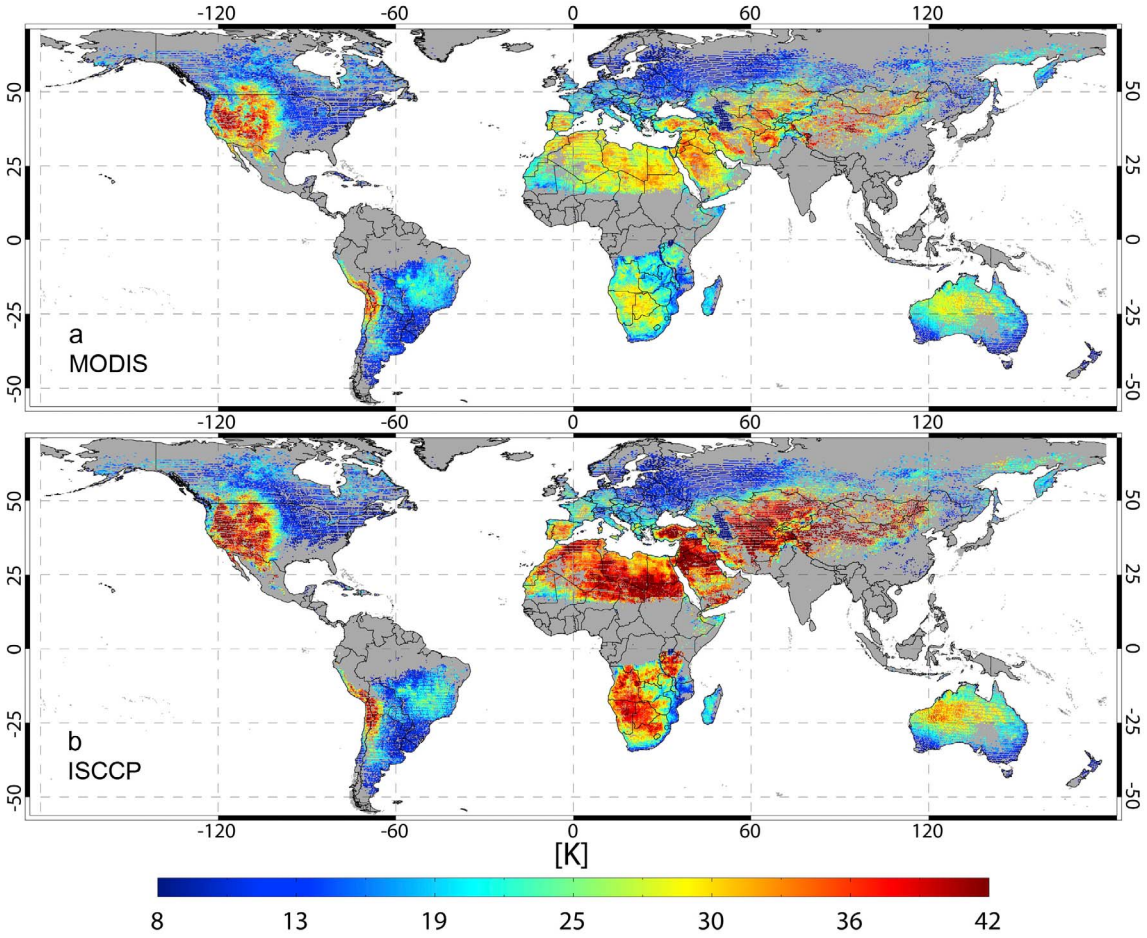

Figure 4. Monthly average diurnal LST amplitude (day minus night) from (a) MODIS and (b) ISCCP, for clear conditions during July 2003.

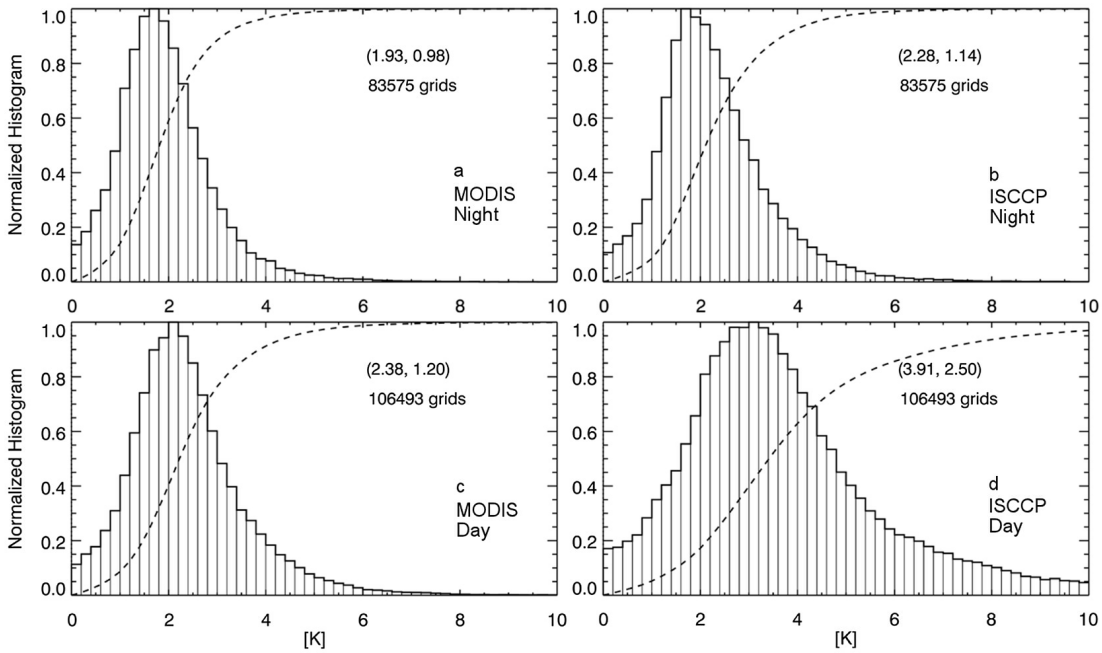

Figure 5. Histograms of standard deviations of LST from (a and c) MODIS and (b and d) ISCCP for night (Figures 5a and 5b) and day (Figures 5c and 5d) measurements for July 2003. The mean and standard deviation are in parentheses.

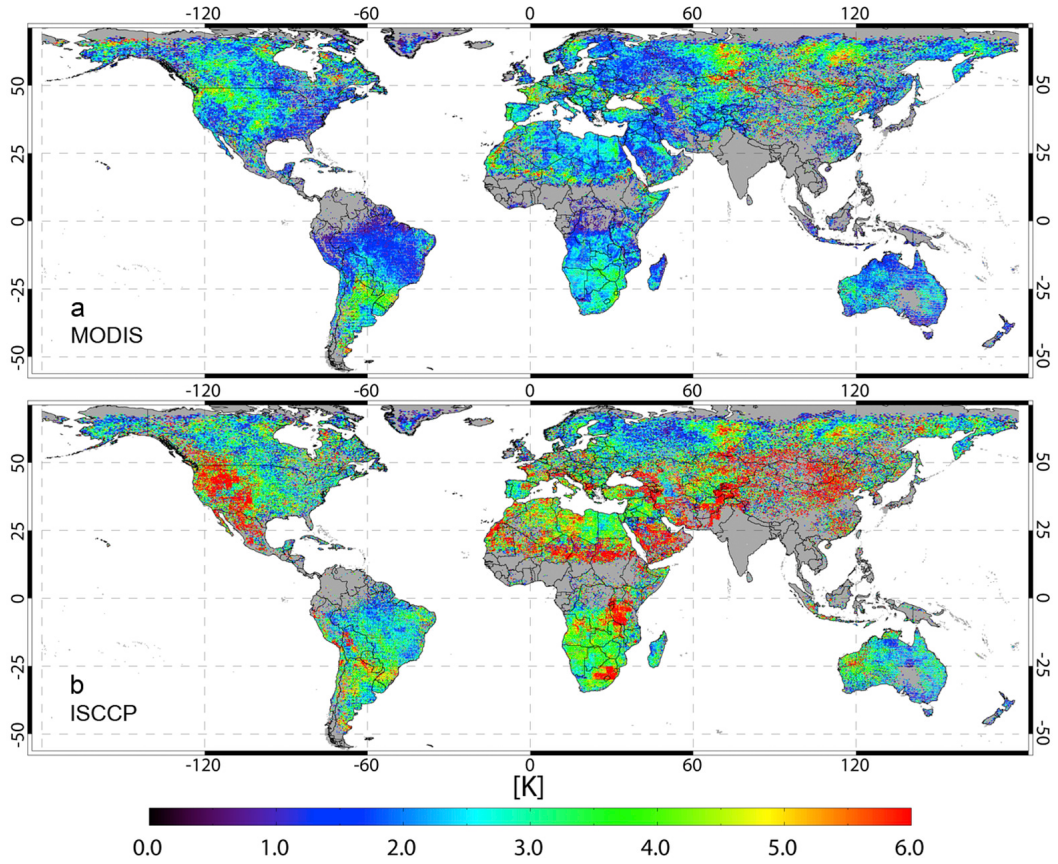

Figure 6. Standard deviations of LST from (a) MODIS and (b) ISCCP for day measurements for July 2003. Areas with missing data are in gray.

[16] Errors due to time interpolation of the ISCCP LSTs to the MODIS measurement time are expected to be significant at midday, especially over desert, when a linear interpolation produces a value lower than the true peak LST. These interpolation errors add to the temporal standard deviation because of the daily shift in the spacecraft orbit compared to a fixed reference on Earth, which in turn causes a given location to be viewed at different times from day to day (in different lateral positions in the MODIS swath). Figure 7 shows day and night scatterplots of the ISCCP-MODIS LST differences versus the difference between the MODIS time of overpass and the nearest bracketing time of the ISCCP data, $\Delta t_{MODIS\text{-}ISCCP}$. In the day plot, the mean ISCCP-MODIS LST difference is maximum at $\Delta t_{MODIS\text{-}ISCCP} = 0$, where time interpolation errors vanish, and decreases by 2–3K at $\Delta t_{MODIS\text{-}ISCCP} = \pm 1.5$ hr. This pattern is consistent with an overall positive difference overlaid with a smaller negative interpolation error. There is no clear trend in the scatter of LST difference versus $\Delta t_{MODIS\text{-}ISCCP}$. For night data, the differences are slightly higher (~1 K) for $\Delta t_{MODIS\text{-}ISCCP} = \pm 1.5$ than at the center, which is consistent with the positive interpolation error expected for a broad local minimum in LST. The large amount of scatter in the MODIS-ISCCP LST differences for any given value of $\Delta t_{MODIS\text{-}ISCCP}$ is clearly due to discrepancies between the MODIS and ISCCP LST products from other causes. Considering the comparatively small magnitude of the interpolation bias, this effect is expected to have only a secondary impact on the histograms of ISCCP-MODIS LST differences (Figure 3). Over persistently clear areas, the time interpolation errors are negative in the daytime, so elimination of these errors would amplify the already high mean daytime ISCCP-MODIS differences over deserts.

[17] One possible source of differences in temporal variability between MODIS and ISCCP LST is error in LST retrieval arising from errors in ancillary variables such as cloud cover. Any cloud contamination of the "clear" LST reports would increase LST standard deviation because cloud radiative effects tend to vary greatly from day to day. Conversely, if cloud screening is overly conservative, it might exclude uncontaminated unusual LSTs and decrease variability. Many areas where ISCCP LST monthly standard deviation is much bigger than MODIS are arid, where cloud errors are unlikely to be a significant factor.

4. Diagnosis With Microwave Emissivity Retrievals

[18] In order to simplify interpretations of consistency between the LST data and the microwave measurements, we were as consistent as possible in our processing of data from different sources: using the methods we had applied to AMSR-E and MODIS also for SSM/I and ISCCP. A careful comparison between the July 2003 F13 and F15 SSM/I

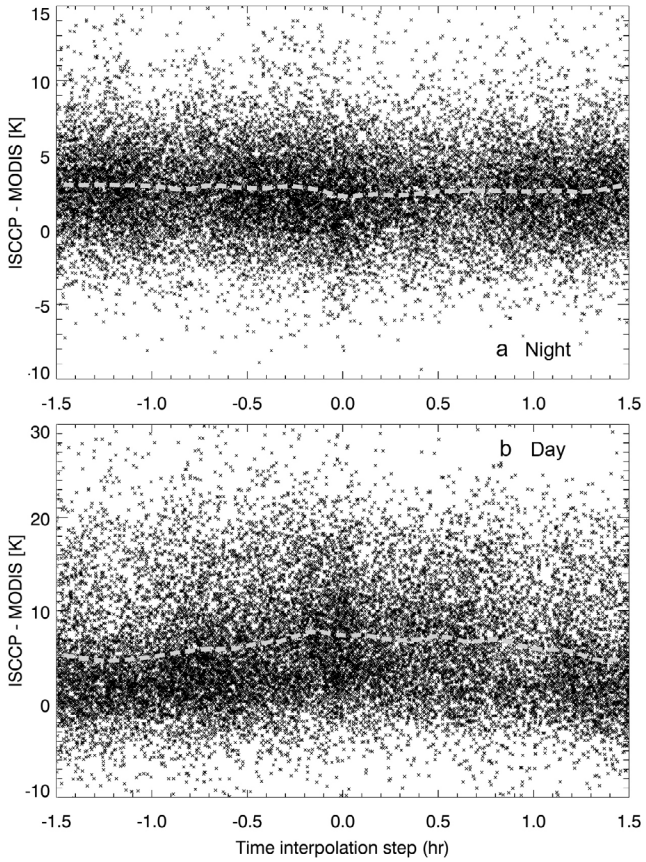

Figure 7. ISCCP-MODIS LST differences as a function of $\Delta t_{MODIS\text{-}ISCCP}$ (as defined in the text) for (a) night and (b) day, for July 2003. The dashed lines mark the averages (at 4.5-min increments).

emissivities generated for this analysis and those produced separately by *Prigent et al.* [1997] showed good agreement between the two SSM/I products, providing a form of validation of the numerical processes and, as a by-product, a finding that the retrieved monthly mean emissivities were not very sensitive to differences in the details of the implementation and ancillary data processing.

[19] Consistency of the MODIS and ISCCP-derived LST with AMSR-E measurements is affected not only by intrinsic differences in the error characteristics of the two LST products, but also by errors introduced in the temporal and spatial matching of the ISCCP product to AMSR-E. The temporal matching factor was discussed in section 3 in the context of direct comparisons between ISCCP and MODIS LST products. The results shown in this section indicated that time interpolation errors are not the primary cause for the higher temporal variability of the ISCCP LST. Spatial interpolation errors would generally be largest when solar heating is high (e.g., near the AMSR-E ascending overpass), because of the larger degree of spatial inhomogeneity in LST, as surface properties modulate the response to radiative fluxes. Spatial interpolation errors would tend to be larger for ISCCP than for MODIS because our ISCCP processing started from LST pre-averaged over a 30-km grid, whereas our MODIS processing started with the 5-km products. In our process, spatial interpolation error impacts on ESD are reduced by the averaging of emissivity from multiple microwave footprints to a fixed grid for each satellite overpass.

[20] To eliminate most natural changes in surface properties as a potential cause of microwave emissivity temporal variability and to avoid potential artifacts of differences among the Aqua and DMSP satellites with respect to temporal sampling of highly variable surfaces, we restricted this analysis to locations with low standard deviation of AMSR-E. R11 = T^B_{11H}/T^B_{11V}. The R11 polarization ratio is essentially insensitive to variations in atmospheric state (outside of precipitation) and surface temperature, leaving changes in surface physical properties as the main factor modulating the R11 time series [*Moncet et al.*, 2011]. Figure 8 shows examples of impacts of changes in soil moisture (due to precipitation or surface water runoff) or vegetation cover on the R11 time series [*Moncet et al.*, 2011]. This screen also eliminates areas of high spatial inhomogeneity.

[21] The 19-GHz frequency was chosen for the global analysis of temporal consistency of microwave measurements with MODIS and ISCCP LST because it is the lowest frequency common to these sensors, and thus it has the lowest sensitivity to cloud liquid water and its temporal variations. The emissivities were obtained using the formula (1) in which LST is treated as an approximation of $T_{eff,\nu}$, without excluding arid regions.

[22] Emissivities retrieved from descending and ascending orbits tend to have opposite biases in arid regions due to microwave surface penetration in the presence of day–night differences in subsurface thermal gradients [*Moncet et al.*, 2011; *Galantowicz et al.*, 2011]. When ignoring penetration effects and using infrared skin temperature for T_{eff} at all frequencies in the process of retrieving surface emissivity from observed brightness temperatures, it results an apparent change in surface emissivity from day to night, the retrieved emissivities being biased low during the day and high at night. In order to prevent these biases from artificially broadening the ESD histograms we kept separate statistics for the descending and ascending satellite passes. Nevertheless, there is a secondary effect in high-penetration areas wherein ESD could be inflated when there is temporal instability (within the monthly time scale) of the thermal forcing at the surface, which would cause temporal variations in the subsurface thermal gradients. While we have not quantified this secondary effect on ESD, we infer that it would be a larger factor for AMSR-E than for SSM/I because the primary effect of penetration on emissivities retrieved with (1)—differences between the ascending and descending products—were larger for AMSR-E than for SSM/I [*Galantowicz et al.*, 2011].

[23] The ESD_{19H} histograms obtained with our process for AMSR-E and DMSP F13 and F15 SSM/I (not shown) are consistent with those shown in Figure 1. The histograms for AMSR-E for July 2003 are substantially narrower and peak at lower values than the SSM/I histograms. Table 1 provides the fraction of grid points with $ESD_{19H} < 0.01$ for the three sensors. It is apparent from this table that this fraction is substantially lower for SSM/I than for AMSR-E.

[24] Further investigation revealed that the higher temporal variability of the SSM/I emissivity estimates, relative to AMSR-E, is largely explained by differences between the

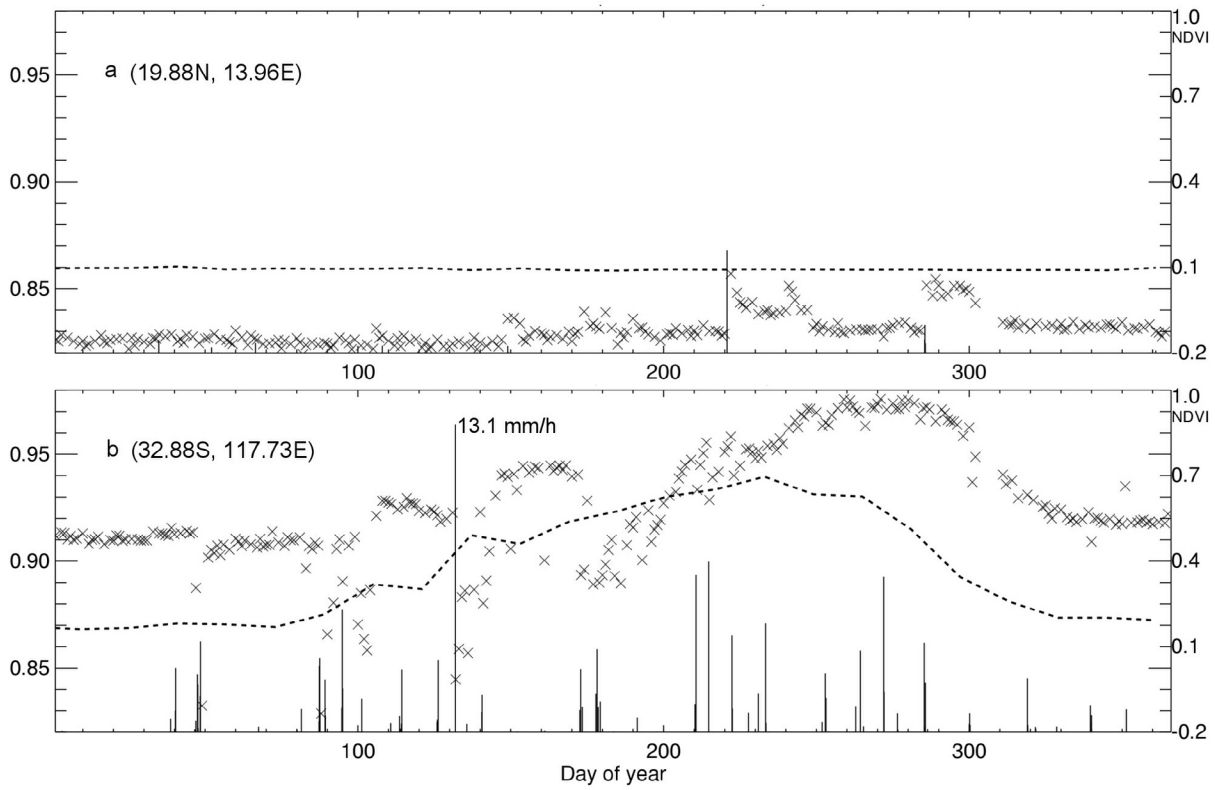

Figure 8. Examples of R11 time series (crosses) over (a) Northern Niger (sand desert) and (b) South Western Australia (cropland) showing impact of changes in soil moisture and vegetation cover. Precipitation amounts from Tropical Rainfall Measuring Mission (TRMM) interpolated to the times and locations of the gridded AMSR-E measurements are overlaid on these plots. Vertical bars in both panels are plotted on the same scale, indicated by the maximum of 13.1 mm/hr reached on day 132 over Australia. Dotted lines represent the Normalized Difference Vegetative Index (NDVI) from the 16-day MYD13A2 MODIS product. The Australian location in Figure 8b failed our stability test for the month of July (days 182–212).

ISCCP and MODIS-derived LST. This finding was obtained by comparing AMSR-E 19H emissivities retrieved using ISCCP LST with those obtained using MODIS LST. Only clear AMSR-E emissivity estimates, per both MODIS and ISCCP criteria, were included in this comparison. It is apparent from maps (Figure 9) and histograms (Figure 10) that the AMSR-E ESD degrade significantly when LST is from ISCCP rather than MODIS, indicating that the temporal consistency between AMSR-E brightness temperatures and the infrared-derived LST is lower for ISCCP than for MODIS. As expected based on the results in Figure 5, the ESD_{19H} retrieved from these two LST sources differ more in the daytime than at night. Moderate degradation of ESD when switching from MODIS to ISCCP (positive differences in Figure 9) is quite widespread, and affects densely vegetated and arid regions.

[25] Another way to assess LST consistency is by considering the day–night differences in retrieved emissivities. The actual emissivities are expected to be nearly identical between day and night. In arid regions, and especially in sandy deserts [*Prigent et al.*, 1999], the biases in retrieved emissivities (due to microwave penetration, as discussed above) tend to give negative day–night differences [*Moncet et al.*, 2011; *Galantowicz et al.*, 2011]. We present results for the 89V channel because microwave penetration is less at the higher frequencies, and thus anomalies are easier to discern. The specific areas analyzed here were selected among the areas with temporally stable surface properties, in arid and semi-arid regions, and with the largest number of clear days, to minimize chances of residual cloud liquid water contamination at 89 GHz and the impact of cloud/dust contamination of the LST products.

[26] Maps of day–night emissivity differences computed with ISCCP -derived LST (Figures 11c and 11d) are much noisier than the corresponding MODIS maps (Figures 11a and 11b). The ISCCP maps over Southern Africa have a predominance of areas with differences characteristic of deep microwave penetration, including Angola and Northwestern

Table 1. Fraction of Grid Points With July 2003 ESD_{19H} Less Than 0.01 for Clear AMSR-E and SSM/I Measurements Over Homogeneous Stable Surfaces

	Time	Fraction
AMSR-E	Night	0.91
AMSR-E	Day	0.91
SSM/I F13	Evening	0.63
SSM/I F13	Morning	0.65
SSM/I F15	Evening	0.68
SSM/I F15	Morning	0.51

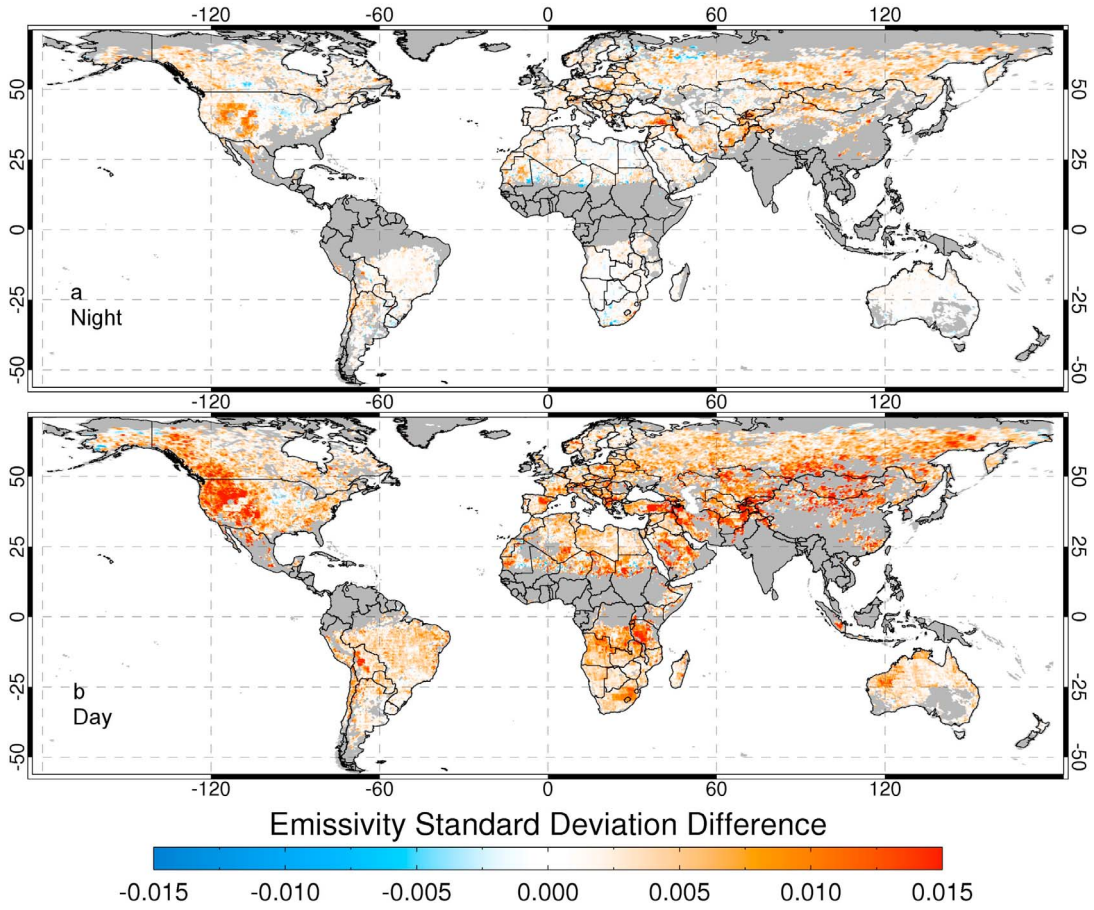

Figure 9. Differences between AMSR-E ESD_{19H} produced with ISCCP and with MODIS LST, for (a) night and (b) day measurements from temporally stable clear ($F_{clear} \geq 98\%$) conditions in July 2003.

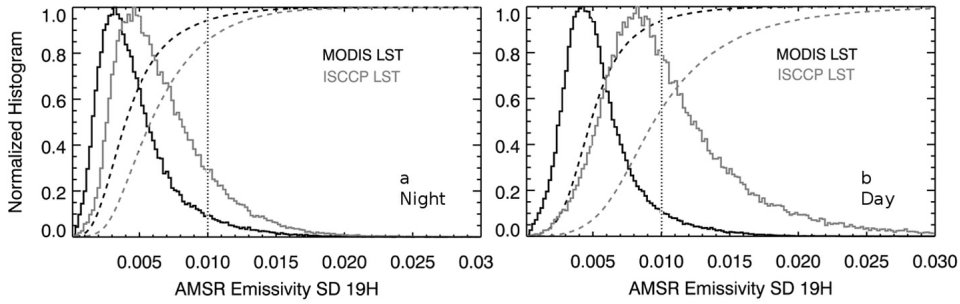

Figure 10. Histograms of AMSR-E 19H ESD produced with MODIS (black) and ISCCP (gray) LST, for (a) night and (b) day measurements from temporally stable ($\sigma_{R11} < 0.01$) clear ($F_{clear} \geq 98\%$) conditions in July 2003. The cumulative frequency distributions are dashed.

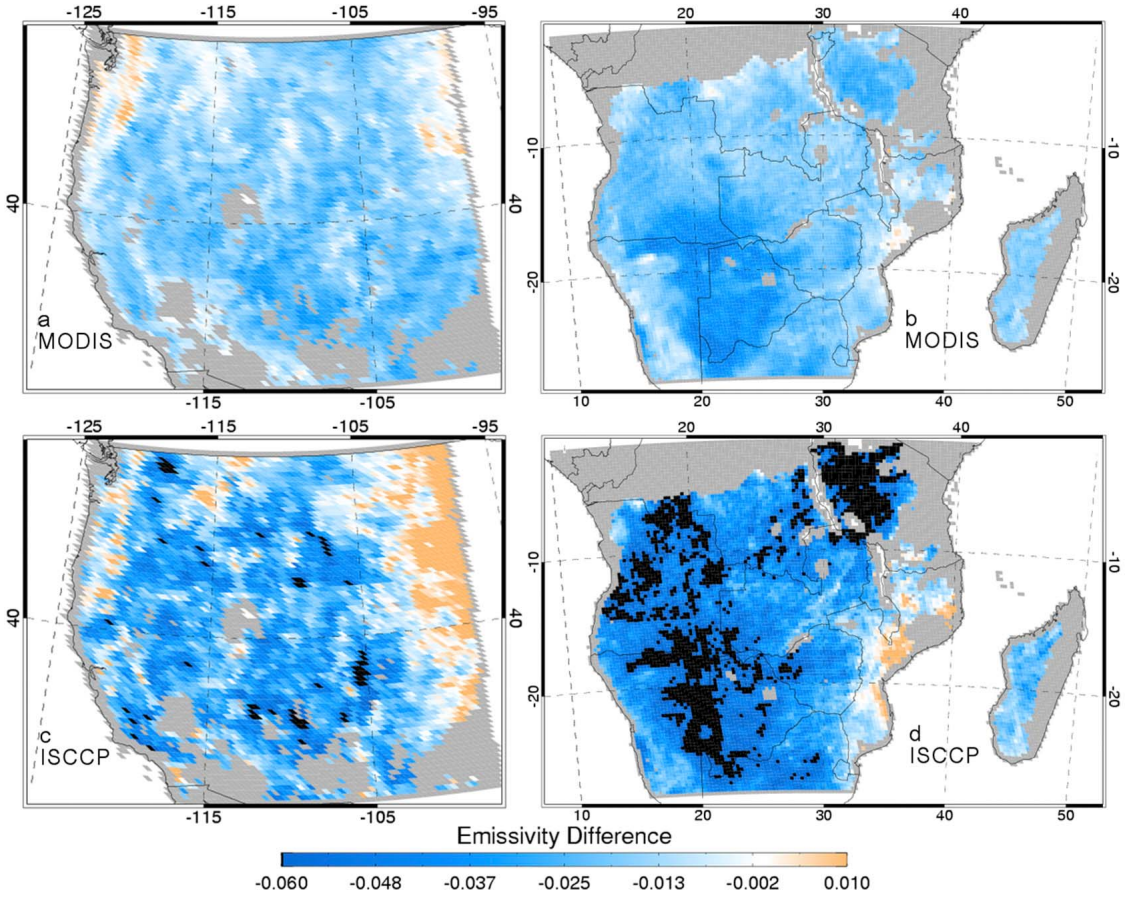

Figure 11. Maps of monthly averaged 89V day–night emissivity difference from (a and b) MODIS and (c and d) ISCCP, for temporally stable ($\sigma_{R11} < 0.01$) clear ($F_{clear} \geq 98\%$) conditions in July 2003. The Western U.S. (Figures 11a and 11c) and Southern Africa (Figures 11b and 11d) are shown.

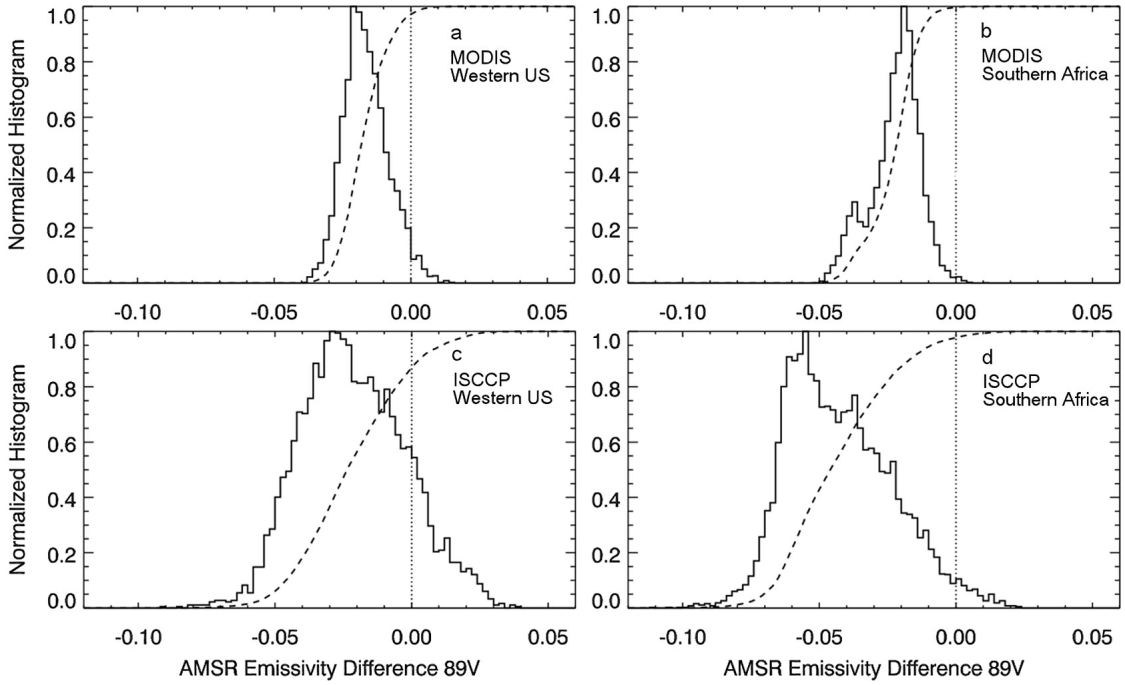

Figure 12. Histograms of monthly averaged 89V day–night emissivity difference from (a and b) MODIS and (c and d) ISCCP, for temporally stable ($\sigma_{R11} < 0.01$) clear ($F_{clear} \geq 98\%$) conditions in July 2003. The regions represented correspond to the maps in Figure 11.

Tanzania, regions that are not classified as deserts. Considering these and other regions, we observed that large negative day–night differences in arid regions appear to be more extensive with ISCCP than they are with MODIS as the source of LST. This is consistent with the fact that, in these regions, the daytime ISCCP LST values are much higher than those from MODIS (Figure 2).

[27] The histograms of day–night emissivity differences computed with MODIS-derived LST have a primary mode peaking in the range [−0.01, −0.02] in arid and semi-arid regions (Figures 12a and 12b), indicating a predominance of surfaces with relatively little penetration at 89 GHz in these regions. The fact that the primary peak is quite narrow over the Western U.S., and Southern Africa (and other areas not shown here) indicates that the relationship (in a monthly average sense) between day and night AMSR-E brightness temperatures and MODIS LST is remarkably similar between different grid points within a region and across geographically distinct regions. By comparison, the ISCCP histograms (Figures 12c and 12d) are much broader and contain a significant fraction of positive day–night emissivity differences.

[28] The evidence from these analyses point toward substantial local biases in the ISCCP-derived diurnal LST amplitudes causing some anomalies and inconsistencies in the AMSR-E day–night emissivity differences. This result may be related to the observation that there is large temporal variability in the day ISCCP LST data at individual locations (Figure 5d).

5. Conclusion

[29] Comparisons of LST products from MODIS and ISCCP infrared data indicate that there are very significant, systematic discrepancies between the data sets. We found the discrepancies were larger in arid and semi-arid regions than in more heavily vegetated regions, and were larger midday (13:30 LT) than midnight (01:30 LT). For July 2003 monthly averages, the ISCCP-MODIS differences were 5.0 K and 2.5 K for day and night, respectively, in terms of averages over all clear-sky locations. The day differences were as large as 25 K for the monthly average. The maximum positive differences over arid regions are qualitatively consistent with comparisons of ISCPP LST with outgoing longwave radiation measurements [*Tsuang et al.*, 2008]. The day–night differences, an approximation of the amplitude of the average diurnal cycle, were as much as ~10 K higher for ISCCP than for MODIS. These discrepancies are large enough that, when LST data are applied to weather or climate model assimilation or analysis (for example), the selection of LST data set could have a quite significant effect on the findings.

[30] We found considerable evidence that the MODIS LST data were generally more precise and more accurate than those from ISCCP. The temporal variability in retrieved LST over the course of the month was lower for MODIS than for ISCPP in clear-sky areas at midday. While we do not know the true temporal variability of LST in these regions, the plausible error sources are more likely to cause the variability to be erroneously inflated than suppressed. Independent microwave measurements from AMSR-E were much more consistent with the LST from MODIS than from ISCCP, with respect to temporal variations and the amplitude of the diurnal cycle. The method of analysis took account of the differences between the microwave and infrared radiative properties, wherein clear-sky LST data were used in retrieval of microwave emissivities, and then the emissivities were assessed in terms of temporal stability and consistency with surface

properties. The clarity with which the microwave-infrared combined analysis showed differences between the MODIS and ISCCP products demonstrates the effectiveness this analysis approach for validating LST products. Our innovative application of microwave data serves as a complement to validations against other types of data (such as in situ measurements) performed by the LST data producers.

[31] The analyses presented in this paper focused on the month of July 2003 but analyses performed for the months of June and September yielded qualitatively similar results. The findings of this study indicate that further validation of the ISCCP LST products is warranted and that the ISCCP algorithm for LST retrieval would likely benefit from further development. The ISCCP data set has considerable advantages over MODIS, due to its more extensive diurnal sampling and the longer period of record. One option currently available to ISCCP data users, in applications sensitive to the diurnal cycle amplitude, is to scale the ISCCP products to match the MODIS amplitude. The results of the analysis presented in this paper prompted a separate study aimed at determining the causes for the observed discrepancies between ISCCP and MODIS LSTs. Causes under consideration include sensor calibration issues in the ISCCP product over hot desert surfaces and errors in water vapor specification (C. Prigent, personal communication, 2011).

[32] Subsequent to the performance of the analyses reported here, Version 5 [*Wan*, 2008; *Wan and Li*, 2008] of the MODIS LST product became available. In our limited comparisons of the two versions, we found that the V4 and V5 products generally agree well over vegetated areas but significant differences were observed over arid areas and in particular in the Sahara desert in July 2003. *Hulley and Hook* [2009] also caution about the use of V5 over deserts. However, differences were not large enough to significantly affect the conclusions of this study.

[33] **Acknowledgments.** This paper is based upon work supported by the National Aeronautics and Space Administration under contract NNH04CC43C issued through the Science Mission Directorate. We thank Z. Wan of the University of California at Santa Barbara for providing information about MODIS LST data, and for providing software for cloud filtering. Yuguang He performed software development in support of this work.

References

Aires, F., C. Prigent, and W. B. Rossow (2004), Temporal interpolation of global surface skin temperature diurnal cycle over land under clear and cloudy conditions, *J. Geophys. Res.*, *109*, D04313, doi:10.1029/2003JD003527.

Bosilovich, M. G., J. D. Radakovich, A. Da Silva, R. Todling, and F. Verter (2007), Skin temperature analysis and bias correction in a coupled land-atmosphere data assimilation system, *J. Meteorol. Soc. Jpn.*, *85A*, 205–228, doi:10.2151/jmsj.85A.205.

Coll, C., Z. Wan, and J. M. Galve (2009), Temperature-based and radiance-based validations of the V5 MODIS land surface temperature product, *J. Geophys. Res.*, *114*, D20102, doi:10.1029/2009JD012038.

Colton, M. C., and G. A. Poe (1999), Intersensor calibration of DMSP SSM/I's: F-8 to F-14, 1987–1997, *IEEE Trans. Geosci. Remote Sens.*, *37*, 418–439, doi:10.1109/36.739079.

Galantowicz, J. F., J.-L. Moncet, P. Liang, A. Lipton, G. Uymin, C. Prigent, and C. Grassotti (2011), Subsurface emission effects in AMSR-E measurements: Implications for land surface microwave emissivity retrieval, *J. Geophys. Res.*, *116*, D17105, doi:10.1029/2010JD015431.

Hollinger, J. P., J. L. Peirce, and G. A. Poe (1990), SSM/I instrument evaluation, *IEEE Trans. Geosci. Remote Sens.*, *28*, 781–790, doi:10.1109/36.58964.

Hulley, G. C., and S. J. Hook (2009), Intercomparison of versions 4, 4.1 and 5 of the MODIS Land Surface Temperature and Emissivity products and validation with laboratory measurements of sand samples for the Namib desert, Namibia, *Remote Sens. Environ.*, *113*, 1313–1318, doi:10.1016/j.rse.2009.02.018.

Ignatov, A., and G. Gutman (1999), Monthly mean diurnal cycles in surface temperatures over land for global climate studies, *J. Clim.*, *12*, 1900–1910, doi:10.1175/1520-0442(1999)012<1900:MMDCIS>2.0.CO;2.

Kalnay, E., M. Kanamitsu, and W. E. Baker (1990), Global numerical weather prediction at the National Meteorological Center, *Bull. Am. Meteorol. Soc.*, *71*, 1410–1428, doi:10.1175/1520-0477(1990)071<1410:GNWPAT>2.0.CO;2.

Kanamitsu, M. (1989), Description of the NMC global data assimilation and forecast system, *Weather Forecasting*, *4*, 335–342, doi:10.1175/1520-0434(1989)004<0335:DOTNGD>2.0.CO;2.

Kawanishi, T., T. Sezai, Y. Ito, K. Imaoka, T. Takeshima, Y. Ishido, A. Shibata, M. Miura, H. Inahata, and R. W. Spencer (2003), The Advanced Microwave Scanning Radiometer for the Earth Observing System (AMSR-E), NASDA's contribution to the EOS for global energy and water cycle studies, *IEEE Trans. Geosci. Remote Sens.*, *41*, 184–194, doi:10.1109/TGRS.2002.808331.

Liebe, H. J., P. W. Rosenkranz, and G. A. Hufford (1992), Atmospheric 60-GHz oxygen spectrum: New laboratory measurements and line parameters, *J. Quant. Spectrosc. Radiat. Transfer*, *48*, 629–643, doi:10.1016/0022-4073(92)90127-P.

Lipton, A., J.-L. Moncet, S.-A. Boukabara, G. Uymin, and K. Quinn (2009), Fast and accurate radiative transfer in the microwave with optimum spectral sampling and improved Planck approximation, *IEEE Trans. Geosci. Remote Sens.*, *47*, 1909–1917, doi:10.1109/TGRS.2008.2010933.

Moncet, J.-L., P. Liang, J. F. Galantowicz, A. E. Lipton, G. Uymin, C. Prigent, and C. Grassotti (2011), Land surface microwave emissivities derived from AMSR-E and MODIS measurements with advanced quality control, *J. Geophys. Res.*, *116*, D16104, doi:10.1029/2010JD015429.

Prigent, C., W. B. Rossow, and E. Matthews (1997), Microwave land surface emissivities estimated from SSM/I observations, *J. Geophys. Res.*, *102*, 21,867–21,890, doi:10.1029/97JD01360.

Prigent, C., W. B. Rossow, E. Matthews, and B. Marticorena (1999), Microwave radiometer signatures of different surface types in deserts, *J. Geophys. Res.*, *104*(D10), 12,147–12,158, doi:10.1029/1999JD900153.

Prigent, C., F. Aires, and W. B. Rossow (2006), Land surface microwave emissivities over the globe for a decade, *Bull. Am. Meteorol. Soc.*, *87*, 1573–1584, doi:10.1175/BAMS-87-11-1573.

Rosenkranz, P. W. (1998), Water vapor microwave continuum absorption: A comparison of measurements and models, *Radio Sci.*, *33*, 919–928, doi:10.1029/98RS01182.

Rossow, W. B., and L. C. Garder (1993a), Cloud detection using satellite measurements of infrared and visible radiances for ISCCP, *J. Clim.*, *6*, 2341–2369, doi:10.1175/1520-0442(1993)006<2341:CDUSMO>2.0.CO;2.

Rossow, W. B., and L. C. Garder (1993b), Validation of ISCCP cloud detections, *J. Clim.*, *6*, 2370–2393, doi:10.1175/1520-0442(1993)006<2370:VOICD>2.0.CO;2.

Rossow, W. B., and R. A. Schiffer (1999), Advances in understanding clouds from ISCCP, *Bull. Am. Meteorol. Soc.*, *80*, 2261–2287, doi:10.1175/1520-0477(1999)080<2261:AIUCFI>2.0.CO;2.

Tsuang, B.-J., M.-D. Chou, Y. Zhang, A. Roesch, and K. Yang (2008), Evaluations of land-ocean skin temperatures of the ISCCP satellite retrievals and the NCEP and ERA reanalyses, *J. Clim.*, *21*, 308–330, doi:10.1175/2007JCLI1502.1.

Wan, Z. (1999), MODIS land-surface temperature algorithm theoretical basis document, version 3.3, report, NASA Goddard Space Flight Cent., Greenbelt, Md. [Available at http://modis.gsfc.nasa.gov/data/atbd/atbd_mod11.pdf.]

Wan, Z. (2008), New refinements and validation of the MODIS land-surface temperature/emissivity products, *Remote Sens. Environ.*, *112*, 59–74, doi:10.1016/j.rse.2006.06.026.

Wan, Z., and Z.-L. Li (2008), Radiance-based validation of the V5 MODIS land-surface temperature product, *Int. J. Remote Sens.*, *29*, 5373–5395, doi:10.1080/01431160802036565.

Wan, Z., P. Wang, and X. Li (2004a), Using MODIS land surface temperature and normalized difference vegetation index for monitoring drought in the southern Great Plains, USA, *Int. J. Remote Sens.*, *25*, 61–72, doi:10.1080/0143116031000115328.

Wan, Z., Y. Zhang, Q. Zhang, and Z.-L. Li (2004b), Quality assessment and validation of the MODIS global land surface temperature, *Int. J. Remote Sens.*, *25*, 261–274, doi:10.1080/0143116031000116417.

Wang, K., Z. Wan, P. Wang, M. Sparrow, J. Liu, X. Zhou, and S. Haginoya (2005), Estimation of surface long wave radiation and broadband emissivity using Moderate Resolution Imaging Spectroradiometer (MODIS) land surface temperature/emissivity products, *J. Geophys. Res.*, *110*, D11109, doi:10.1029/2004JD005566.

Zhang, Y.-C., C. N. Long, W. B. Rossow, and E. G. Dutton (2010), Exploiting diurnal variations to evaluate the ISCCP-FD flux calculations and radiative-flux-analysis processed surface observations from BSRN, ARM and SURFRAD, *J. Geophys. Res.*, *115*, D15105, doi:10.1029/2009JD012743.

J. F. Galantowicz, P. Liang, A. E. Lipton, and J.-L. Moncet, Atmospheric and Environmental Research, 131 Hartwell Ave, Lexington, MA 02421-3126, USA. (jmoncet@aer.com)

C. Prigent, Laboratoire d'Etudes du Rayonnement et de la Matière en Astrophysique, Observatoire de Paris, CNRS, 61, Avenue de l'Observatoire, F-75014 Paris, France.